# Morphological evolution of grain boundaries under lateral strains

Ming-Wei Liu,[1,*] Mogadalai P. Gururajan,[2] and Kuo-An Wu[1,†]
[1]*Department of Physics, National Tsing Hua University, Hsinchu 30013, Taiwan*
[2]*Department of Metallurgical Engineering and Materials Science, Indian Institute of Technology Bombay, Powai Mumbai 400076, India*

(Received 19 August 2021; accepted 28 January 2022; published 11 February 2022)

A theory for the lateral strain-induced grain boundary instability is proposed by considering two crucial factors, namely, the dependence of the boundary energy on coincidence sites and the differences in elastic responses of the grain and the boundary regions. In contrast to the Asaro-Tiller-Grinfeld instability, where strains, however small, lead to breakup of the interfaces and the amplitudes of the perturbations are only a function of wavelength and time, we find that there exists a critical strain for the grain boundary instability to occur which is due to the periodicity of coincidence site lattices, and the growth rate of perturbations is dependent on the amplitude. These theoretical predictions are validated by the phase field crystal simulations in two dimensions. In addition, the amplitude-dependent growth rate gives rise to two distinct outcomes for the late stage evolution predicted by the proposed theory, namely, the grain boundary structural transformation and the dislocation emission, as seen in the phase field crystal simulations. Not only is the predicted oscillatory behavior of the growth rate observed in simulations, but also the phase diagram predicted by the theory is in quantitative agreement with the phase field crystal simulations.

DOI: 10.1103/PhysRevMaterials.6.023601

## I. INTRODUCTION

The grain boundary plays a key role in determining physical, mechanical, and chemical properties of materials [1]. Specifically, the response of grain boundaries to shear stresses is of great practical importance. For example, it is suggested that the grain boundary instability induced by the shear stress can lead to superplasticity in polycrystalline materials [2,3]. Shear coupled boundary migration along with grain boundary sliding is known to enhance ductility of metallic thin films, making them suitable for MEMS and flexible electronic applications [4]. Therefore the instability and the morphological changes of grain boundaries in materials subject to external stresses are of great interest to researchers. While the grain boundary instability induced by shear stresses has been investigated in various materials including zirconium carbide ceramics [5], aluminum, and titanium alloys [6], whether the grain boundary instability can be induced through lateral stresses, especially in pure materials, remains an intriguing question for the reasons outlined below.

A well-known surface instability named the Asaro-Tiller-Grinfeld (ATG) instability, commonly seen in epitaxial thin films [7,8] and self-assembled quantum dots [9–11], is induced by lateral strains [12,13]; for this instability to occur, the adjacent solids should be elastically inhomogeneous [14]. The inhomogeneity of elastic moduli of adjacent phases makes it possible for the system to reduce its elastic energy drastically through undulations of the boundary surface. However, for grain boundaries in pure materials, adjacent solids share the same elastic properties; hence, the instability would be inhibited if one only considers elasticity of adjacent phases. Nevertheless, in this paper we show that by considering the elasticity of the grain boundary, even without elastic inhomogeneity of adjacent phases, the planar grain boundary surface can become unstable as the lateral stress exceeds a threshold value for pure materials, and the proposed instability mechanism is validated using the phase field crystal (PFC) simulations [15,16] in two dimensions. In addition, we show the oscillatory amplitude-dependent growth as a direct consequence of the underlying periodic coincidence site lattices. Furthermore, at the late stage of evolution, the PFC model further shows details of the structural change of the grain boundary, nucleation of dislocations, and faceted surface profiles that are closely associated with atomistic arrangement of lattices.

The paper is organized as follows: In Sec. II we consider key ingredients such as elasticity of solid grains and the grain boundary, and the periodicity of the grain boundary energy due to underlying lattices, to formulate a theoretical model for the grain boundary instability subject to lateral strains. A nonlinear evolution equation for the amplitude of the undulation of the grain boundary is derived from the proposed model to investigate the dynamics of the grain boundary instability. Our theory predicts the existence of a critical strain above which the instability occurs and an oscillatory growth behavior during the evolution. In Sec. III we perform PFC simulations of a bicrystal subject to lateral strains in two dimensions. Not only are our theoretical predictions validated by the PFC simulations, but also the PFC simulation reveals more details of two possible outcomes predicted by the theory at late stage evolution, namely, the grain boundary structural transformation and the dislocation emission. Detailed analysis

*mwliu2@illinois.edu
†kuoan@phys.nthu.edu.tw

 

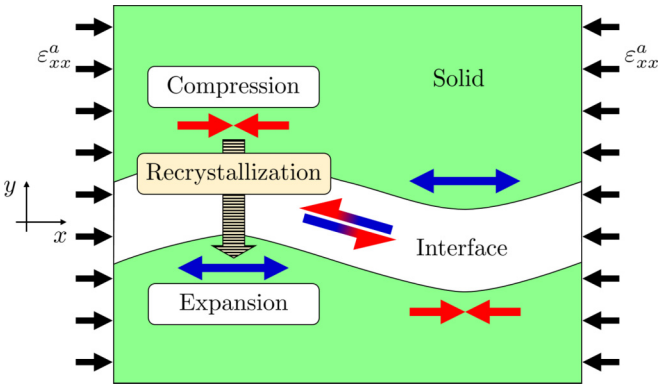


FIG. 1. The schematic plot for the grain boundary instability under applied lateral strains. The red (blue) arrows indicate compressions (expansions) of local lattices as the bicrystal is subject to a lateral compressive strain. The arrows placed in the interface region indicate the direction of shear strains.

of the oscillatory behavior of the growth rate and the phase diagram is discussed, and the theory and PFC simulations are shown to be in quantitative agreement.

## II. THEORETICAL MODEL FOR GRAIN BOUNDARY INSTABILITY

A schematic plot illustrating the grain boundary instability is shown in Fig. 1. Note that the grain boundary itself is an elastic medium composed of a rather disordered and loose atomistic structure compared to bulk solids, which suggests an elastically softer grain boundary layer being sandwiched by solids. Therefore one would expect the instability since the solid phase can bulge into a softer grain boundary region, and the elastic energy difference associated with a curved grain boundary would force the solid to dissolve on one side and to recrystallize on the other side of the grain boundary. To be more specific, the peak regime of one grain has a lower elastic energy density, since the solid can adjust its lattice spacing into a softer grain boundary region while the trough regime is associated with a higher elastic energy density. Therefore the materials in trough regimes on one side of the grain boundary would transform and recrystallize into peak regimes on the other side, which leads to the motion of the grain boundary and the instability.

A theoretical model for the grain boundary instability in pure materials is proposed as follows. For simplicity we consider a two-dimensional system composed of two semi-infinite misoriented solid grains in contact with each other at $y = 0$ that forms a symmetric tilt grain boundary. There is not only the excess interfacial energy (i.e., the grain boundary energy) associated with the grain boundary layer but also the elastic energy. A homogeneous lateral strain parallel to the grain boundary is uniformly imposed to the system, which serves as a driving force to destabilize the planar grain boundary. The elasticity of the bulk solid is assumed to be linear and isotropic, and the elastic energy is

$$F^S_{el} = \int_S \frac{1}{2}(\lambda\varepsilon_{\alpha\alpha}\varepsilon_{\beta\beta} + 2\mu\varepsilon_{\alpha\beta}\varepsilon_{\alpha\beta})\, d\vec{r}, \tag{1}$$

where the subscript $S$ denotes the integration over solid grains, $\lambda$ and $\mu$ are the Lamé constants of solids, and $\varepsilon_{\alpha\beta}$ is the strain field related to the displacement field $u_\alpha$, that is, $\varepsilon_{\alpha\beta} = \frac{1}{2}(\frac{\partial u_\beta}{\partial r_\alpha} + \frac{\partial u_\alpha}{\partial r_\beta})$. Note that the strain field $\varepsilon_{\alpha\beta}$ is composed of the uniform applied strain $\varepsilon^a_{\alpha\beta}$ and the strain field $\varepsilon^u_{\alpha\beta}$ associated with the undulation of the grain boundary, $\varepsilon_{\alpha\beta} = \varepsilon^a_{\alpha\beta} + \varepsilon^u_{\alpha\beta}$. Since we consider the grain boundary as a rather disordered and softer phase sandwiched by solids, when nearby grains exhibit relative motion along the grain boundary, there is a local shear stress in the grain boundary region,

$$\sigma_{tn} = \mu_I \Delta u_t, \tag{2}$$

where $\mu_I$ is the effective interfacial shear modulus, the subscript $t$ ($n$) stands for the tangent (normal) direction with respect to the interface, and $\Delta u_t$ is the relative motion along the interface of two grains. The corresponding interfacial elastic energy is

$$F^I_{el} = \int_I \frac{1}{2}\mu_I \Delta u_t^2\, d\ell, \tag{3}$$

where the integration is along the interface, and $d\ell$ stands for the infinitesimal segment of the interface.

In addition to the elastic energy, the grain boundary also possesses an excess interfacial energy. Usually, for the sake of simplicity the grain boundary energy is treated to be independent of interface position. However, the atomistic arrangement at the grain boundary is not homogeneous but varies as the grain boundary is traversed. Therefore the grain boundary energy $\gamma$ should be a function of the grain boundary position $y_{gb}$, that is,

$$F_{\text{int}} = \int_I \gamma(y_{gb})\, d\ell. \tag{4}$$

The function $\gamma$ is uniquely determined by the underlying bicrystal structure using the coincidence site lattice (CSL) method described in Ref. [17]. To be more specific, the periodicity of the bicrystal structure of symmetric tilt grain boundaries leads to a periodic function $\gamma$ of $y$, that is, $\gamma(y) = \sum_{n=0}^{\infty} \gamma_n \cos(\frac{2n\pi y}{L_{cs}})$, where $L_{cs}$ is the minimum distance in the $y$ direction the grain boundary has to move so that the plane of the CSL repeats. In the following discussion, we retain only $\gamma_0$ and $\gamma_1$ for $\gamma(y)$, which captures the essence of the boundary energy and the influence of CSL on the boundary energy. Subsequently, $\gamma(y)$ exhibits a washboardlike potential along the $y$ direction.

Since the mechanical relaxation of displacement fields is much faster than mass diffusion, the system reaches mechanical equilibrium at all times over the diffusion timescale. The elastic fields within the bulk solid simply follow the mechanical equilibrium condition, $\partial\sigma_{\alpha\beta}/\partial r_\beta = 0$. Together with Eq. (2), one readily obtains the strain fields in solids for a given profile of grain boundary interface. For an undulating grain boundary of a sinusoidal profile, $y_{gb}(x) = A\, e^{ikx} + \text{c.c.}$, the strain fields in solids are

$$\varepsilon_{xx}(x, y_\pm) = \varepsilon^a_{xx} \pm \frac{2\varepsilon^a_{xx} kA}{1+4\mu_I/(Ek)}\left[1 \mp \left(\frac{1+\nu}{2}ky_\pm\right)\right] e^{\mp ky_\pm} e^{ikx} + \text{c.c.}, \tag{5}$$

where c.c. represents the complex conjugate, $y_+$ and $y_-$ are the $y$ coordinate in solids above and below the grain boundary, respectively. $\varepsilon^a_{xx}$ is the lateral applied strain; $\nu$ and $E$ are the Poisson's ratio and the Young's modulus, which are related to the Lamé constants of solids by $\nu = \lambda/(2\mu+\lambda)$ and $E = 4\mu(\mu+\lambda)/(2\mu+\lambda)$ for two-dimensional (2D) isotropic materials. The detail derivation of the strain fields is shown in Appendix A. The strain fields result in a free energy difference across the boundary ($y = 0$),

$$\Delta f_{el} \simeq -\sigma^a_{xx}\Delta\varepsilon_{xx} = -\frac{4E\,{\varepsilon^a_{xx}}^2 kA}{1+4\mu_I/(Ek)}e^{ikx} + \text{c.c.}, \quad (6)$$

which serves as a driving force to destabilize the flat boundary. We can now determine the stability of a planar grain boundary by considering both the elastic and surfaces energies. The migration of the grain boundary is driven by the local free energy difference, namely,

$$\frac{\partial y_{gb}}{\partial t} \simeq -\Gamma\left(\Delta f_{el} + \frac{\delta F_{\text{int}}}{\delta y_{gb}}\right), \quad (7)$$

where $\Gamma$ is the mobility of the grain boundary, and $\delta F_{\text{int}}/\delta y_{gb} \simeq -\gamma y''_{gb} + \partial\gamma/\partial y_{gb}(1+{y'_{gb}}^2/2)$ when $|A|k \ll 1$. For a sinusoidal grain boundary interface assumed above, the resulting evolution equation for $A$ is

$$\frac{\partial A}{\partial t} \simeq -\Gamma\left\{-\frac{4E\,{\varepsilon^a_{xx}}^2 k}{1+4\mu_I/(Ek)} + [\gamma_0+\gamma_1 J_0(\eta)]k^2 - \gamma_1\left(\frac{2\pi}{L_{cs}}\right)^2[J_0(\eta)+J_2(\eta)]\right\}A, \quad (8)$$

where $J_0$ and $J_2$ are Bessel functions, and $\eta \equiv 4\pi|A|/L_{cs}$; see the Appendix B for the detailed derivation. The first term on the right-hand side comes from the local elastic energy difference across the interface as described above. The second term is the surface energy that tends to flatten the interface. The third term is closely related to the additional energy cost or reduction when the atomistic arrangement of lattices changes as the grain boundary migrates. The instantaneous growth rate of the instability $\sigma$ is then composed of a part depending on the wave number, $\sigma_k$, and a part only depending on the amplitude, $\sigma_A$. That is,

$$\sigma_k = \Gamma\left[\frac{4E\,{\varepsilon^a_{xx}}^2 k}{1+4\mu_I/(Ek)} - \bar{\gamma}k^2\right], \quad \sigma_A = \sigma_0[J_0(\eta)+J_2(\eta)], \quad (9)$$

where $\bar{\gamma} \equiv \gamma_0 + \gamma_1 J_0(\eta)$, and $\sigma_0 \equiv \Gamma\gamma_1(2\pi/L_{cs})^2$. In the early stage of the instability where $|A| \ll L_{cs}$, $\sigma_A$ is approximately $\sigma_0$. Therefore the perturbed grain boundary would either be inhibited or become more unstable, depending not only on $\sigma_k$ but also on the sign of $\sigma_0$, which is determined by the relative position of the grain boundary and the underlying bicrystal structure. Furthermore, there exists a critical applied lateral strain $\varepsilon_c$ above which the instability occurs. For example, if one assumes that $\gamma_1$ is negligible for simplicity, then the instability can only occur when the wave number $k$ is smaller than a critical value $k_c$. That is, by requiring $\sigma_k = 0$, one obtains $k_c = 4E\,{\varepsilon^a_{xx}}^2/\gamma_0 - 4\mu_I/E$. Since $k_c > 0$, one obtains the critical lateral strain to be $\varepsilon_c = \sqrt{\mu_I\gamma_0/E^2}$. This instability is different from the ATG instability in which any finite applied strain would induce instability as long as the adjacent solids are elastically inhomogeneous. In addition, as the amplitude of the surface profile keeps increasing so that $|A|$ is comparable to $L_{cs}$, the growth rate would exhibit oscillatory behavior as a function of the amplitude. The oscillatory nature as a result of the periodicity of the coincidence site lattice would disappear at the late stage of the evolution where $|A| \gg L_{cs}$, since the grain boundary interface goes across repeated CSL planes frequently and the discrete effect due to the atomistic arrangement of atoms averages out, and the growth rate is reduced to $\sigma_k$.

The oscillatory behavior of $\sigma$ gives rise to two interesting scenarios at the late stage of the grain boundary evolution. First, for smaller strains, the growth rate could drop across zero since $\sigma_k$ is small and $\sigma_A$ turns negative as $|A|$ gets larger. Once $\sigma$ reaches zero, the grain boundary stops evolving and a static curved grain boundary is expected. Second, for larger strains, $\sigma_k$ is large enough so that $\sigma = \sigma_k + \sigma_A$ remains positive during the oscillation regardless of the amplitude. In this case, the amplitude of the undulation of the grain boundary increases at the late stage until the stress at the trough exceeds a critical value, and dislocations are expected to form and to travel into the grains to reduce the elastic energy, as seen in the ATG instability of SiGe films [18] and $^4$He films [19].

## III. THE PFC SIMULATIONS AND RESULTS

The PFC simulation is employed to validate the proposed model. The PFC model is an atomistic continuum model that is capable of resolving the atomistic structure of the lattice and the grain boundary [20–28] and describing the elasticity and dislocations of solids [29–34], which are key ingredients of the proposed model. We use the PFC formulation in Refs. [15,16] to investigate the grain boundary instability in a 2D hexagonal lattice. Specifically, we employ $\epsilon = 0.1$ and $\bar{\psi}_s = -0.19$ in the PFC simulations. The misorientation of the bicrystal is chosen to be $\Delta\theta \simeq 21.8^\circ$, and the minimum size of a rectangle that accommodates the corresponding strain-free misoriented grain in the PFC simulation is $(\ell_x, \ell_y) = (19.20, 33.26)$ [35]. The key parameter $L_{cs}$ in the proposed theory is then $\ell_y/2$. The periodic boundary condition is employed in the simulation, and the system dimension is set to be $(L_x, L_y) = (99\ell_x, 111\ell_y)$, with the normal of the grain boundary aligned in the $y$ direction. The extended $y$ dimension is designed to avoid possible grain boundary interactions. The simulation grid size is $4096 \times 4096$, which provides us adequate spatial resolution of $8 \times 8$ grid points per atom. The applied lateral strain $\varepsilon^a_{xx}$ is implemented by adjusting the mesh size $\Delta x \to (1+\varepsilon^a_{xx})\Delta x$. In addition, the stress in the $y$ direction induced by the imposed lateral strain is relaxed by adjusting the mesh size $\Delta y \to (1-\nu\varepsilon^a_{xx})\Delta y$. The 2D hexagonal PFC lattice is elastically isotropic, and its Poisson's ratio $\nu$ is simply $1/3$ due to the sixfold symmetry and the Young's modulus is $E = 0.0307$ [16,36]. For the PFC parameters employed here, the relaxation of elastic fields is much faster than the mass diffusion, which ensures that the system is always at mechanical equilibrium [37].

The dispersion relation is readily obtained by initiating the PFC simulation with the profile of the grain boundary a sinusoidal function of wave number $k$ and small amplitude,

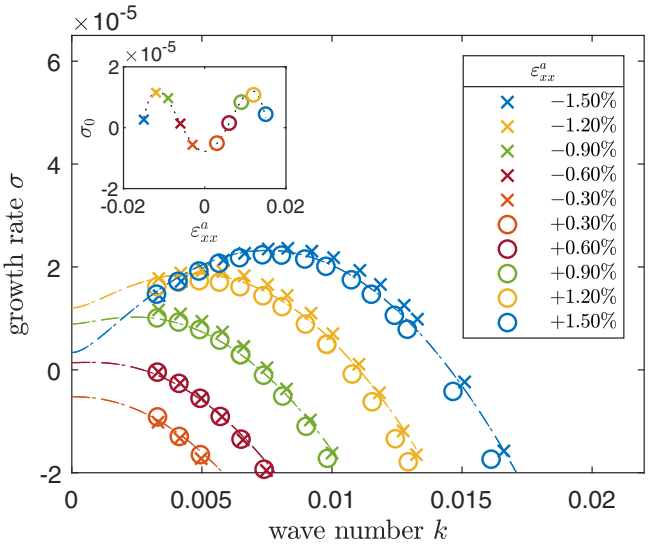


FIG. 2. Dispersion curves for various applied strains $\varepsilon^a_{xx}$ in the limit of $\eta \ll 1$. The PFC simulations are shown in symbols. Crosses and circles represent simulation results for the compressive and tensile applied strains, respectively. The dash-dotted lines are the corresponding theoretical predictions. The inset shows $\sigma_0$ measured from PFC simulations as a function of $\varepsilon^a_{xx}$.

and tracking the evolution of the amplitude. The simulation results are shown in Fig. 2, and dispersion curves measured for various applied strains are in good agreement with the proposed model in the limit where $\eta \ll 1$. The least-squares fitting gives the following physical quantities for the PFC simulation: $\gamma_0 + \gamma_1 = 1.79 \times 10^{-3}$, $\Gamma = 267$, and $\mu_I = 1.04 \times 10^{-5}$. The planar grain boundary is shown to be more unstable when a greater lateral strain is applied. For large strains, the dispersion curves are slightly asymmetric for compressive and tensile strains in PFC simulations. This asymmetry naturally arises from the asymmetric nonlinear elasticity of the PFC lattice as discussed in Ref. [37]. More importantly, in contrast to the ATG instability, there exists a critical applied strain, $\varepsilon_c \simeq 0.445\%$, above which $\sigma_k > 0$, as the proposed model predicts. Furthermore, we discover that $\sigma_0$ is dependent on the applied strain $\varepsilon^a_{xx}$ as shown in the inset of Fig. 2. At small strains $\sigma_0$ is negative, which indicates a stable atomistic structure of a flat grain boundary, and its sign changes around $|\varepsilon^a_{xx}| \simeq 0.545\%$, which suggests that the stable atomistic structure changes due to large strains. Therefore, when the amplitude is small, the grain boundary instability only occurs as its overall growth rate is positive, $\sigma \simeq \sigma_k + \sigma_0 > 0$.

If the instability does occur, when the amplitude is comparable to the lattice parameter, according to the proposed theory, one expects that the grain boundary experiences a washboard potential landscape arising from the repeated structure of the coincidence site lattice, which leads to an oscillatory growth rate. Figure 3 plots the instantaneous growth rate for different wave numbers $k$ observed in PFC simulations with $\varepsilon^a_{xx} = -1.2\%$, which shows the oscillatory behavior at the early stage of the evolution as predicted. To further examine quantitative agreement between our theory and PFC simulations, we compute the strain fields in the PFC simulation by pinpointing accurately the location of each atom and evaluating the corresponding displacement field for each atom. Figure 4 plots the inhomogeneous strain fields induced

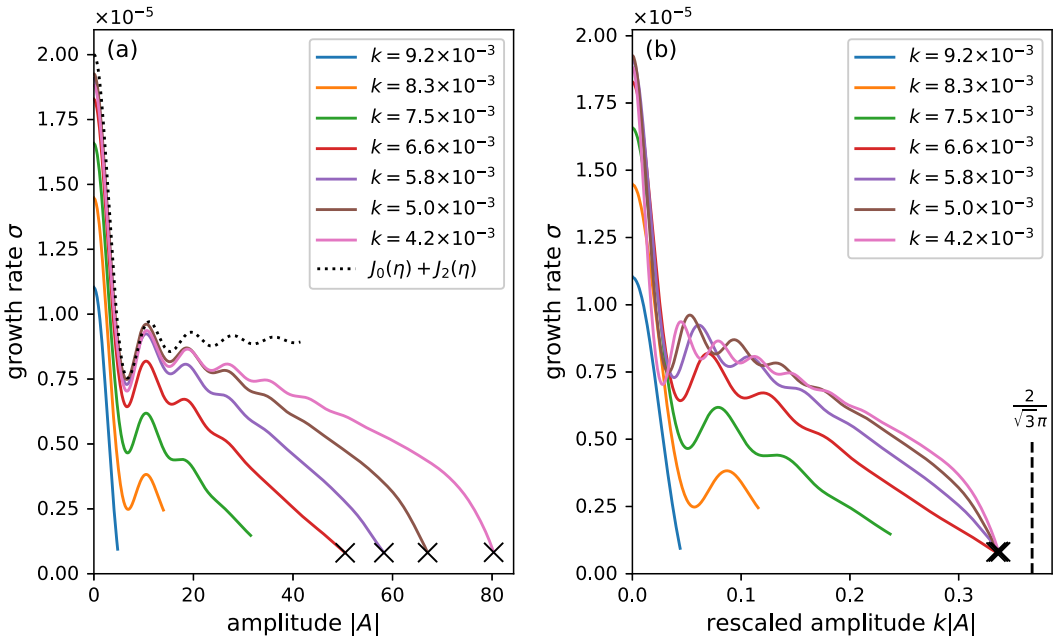


FIG. 3. The instantaneous growth rate for different wave numbers $k$ observed in PFC simulations with $\varepsilon^a_{xx} = -1.2\%$. (a) The growth rate $\sigma$ oscillates with the amplitude $A$. The oscillatory behavior predicted by Eq. (9) is represented by the black dotted curve. The black crosses indicate the moment at which DE happens. (b) With the rescaled amplitude, the occurrences of DE for different $k$'s collapse. The occurrence of DE is close to $k|A| \simeq \frac{2}{\sqrt{3}\pi}$, as indicated with a dashed line, at which the grain boundary forms a faceted triangular wave with the slope of $1/\sqrt{3}$.

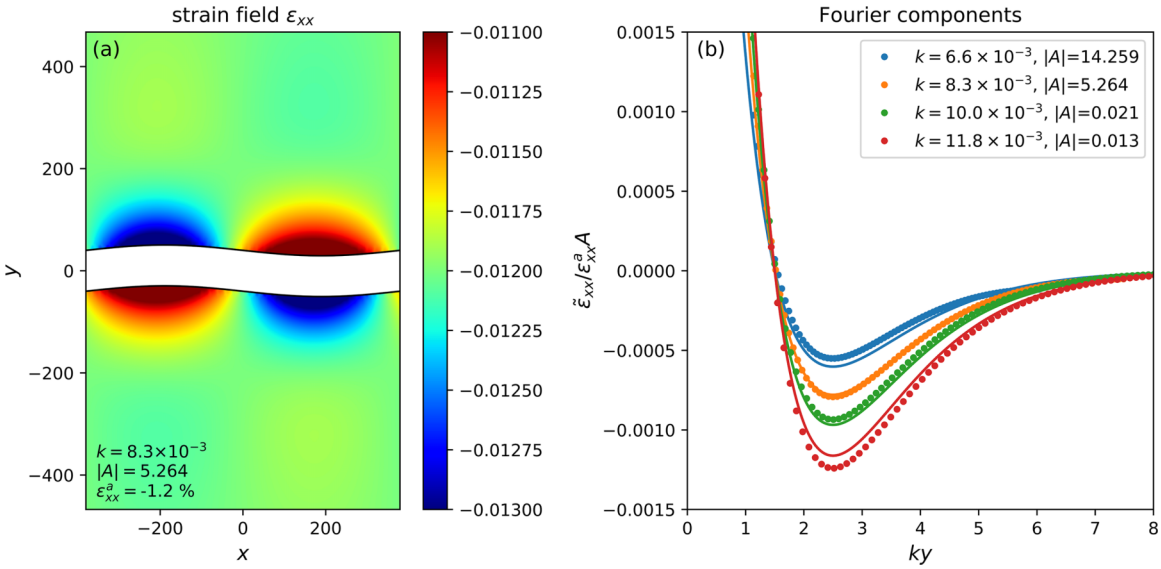


FIG. 4. (a) The inhomogeneous strain field $\varepsilon_{xx}(x, y)$ measured in the PFC simulation with $\varepsilon^a_{xx} = -1.2\%$ induced by the undulating grain boundary of which $|A| \simeq 5.264$ and $k \simeq 8.3 \times 10^{-3}$. Regions subject to compressive and tensile strains are plotted in blue and red, respectively. The region marked by white color indicates the disordered region of the grain boundary, where the strain fields are ill-defined. (b) The Fourier component of $\varepsilon_{xx}$ from PFC simulations with the grain boundary undulations of different wave numbers $k$. The applied strain is $\varepsilon^a_{xx} = -1.2\%$. Note that $\tilde{\varepsilon}_{xx}(y) = \frac{k}{2\pi}\int_0^{2\pi/k} \varepsilon_{xx}(x, y)e^{-ikx}dx$. Dots represent the simulation results and solid curves are the theoretical prediction of Eq. (5).

by the undulating grain boundary of PFC simulations, and the numerical results are in good agreement with the theoretical prediction of Eq. (5).

Two different outcomes at the later stage of evolution, as suggested by the proposed theory, are observed in the PFC simulations. First, as the amplitude of the grain boundary grows, it could eventually saturate to form a steady curved boundary; see first three curves with the wave number above $7.0 \times 10^{-3}$ of PFC simulations in Fig. 3. The growth rate would eventually drop to zero and form a steady curved boundary. Second, the amplitude of the grain boundary could keep growing, and eventually dislocations are nucleated at cusps of the boundary and emit into grains; see curves with the wave number below $7.0 \times 10^{-3}$ of PFC simulations in Fig. 3.

The former case occurs for smaller strains and $\sigma_0 > 0$. In the early stage of evolution, the positive growth rate drives the instability. As the amplitudes grows, the positive growth rate reduces since $\sigma_A$ drops significantly with the amplitude. The amplitudes stop evolving when $\sigma = \sigma_k + \sigma_A$ becomes zero. As shown in the PFC simulations, the atomistic structure of the grain boundary changes for the steady curved boundary, since a positive $\sigma_0$ suggests the atomistic structure of the original planar grain boundary is unstable. This outcome is named the grain boundary structural transformation (GBST). In Fig. 5, an example from the PFC simulations shows that the grain boundary structure undergoes GBST from symmetric kite units to asymmetric zigzag units. The kite units correspond to one of the CSL planes, along which the atomic structures of two misoriented grains match each other. In comparison, the zigzag units do not correspond to perfect CSL planes but approximate CSL planes, along which certain atomic rearrangements are required to match two misoriented grains. Although the zigzag units are energetically unfavorable compared to the kite units in an unstrained system, the zigzag units can be the energetically stable state when applied strain is present.

The latter case occurs for larger strains where not only $\sigma_k + \sigma_0 > 0$ but also $\sigma > 0$ at all times. Hence the growth rate oscillates with the amplitude, but it remains positive regardless of the amplitude. The strain in the grain increases with the amplitude, and dislocations form as the local strain exceeds a threshold; see the PFC simulations shown in Fig. 5. We name this outcome the dislocation emission (DE). Interestingly, in the PFC simulations a morphological change of a curved grain boundary to a faceted one is observed. We see that the grain boundary forms a triangular wave with the slope around 30° as its amplitude becomes pronounced. The faceted grain boundary with a tile angle of 30° corresponds to one of CSL planes as shown in Fig. 5; therefore a planar grain boundary is favored, as the strain is released effectively through nucleation of dislocations at the cusp.

For both cases, the amplitude-dependent growth rates obtained from PFC simulations are in quantitatively good agreement with the proposed theory, as shown in the inset of Fig. 6. Furthermore, the proposed theory can predict the phase boundary between three phases, namely, the stable planar grain boundary, GBST, and DE as follows. The phase boundary between the stable planar grain boundary and the GBST is determined by solving $\sigma(k, \varepsilon^a_{xx}) = 0$ in the limit of $\eta \ll 1$. On the other hand, the phase boundary between the GBST and the DE is determined by requiring $\min(\sigma(\eta)) = 0$. A good approximation for estimating the phase boundary between the GBST and the DE is to look for $\sigma = 0$ in the limit of $\eta \gg 1$. The predicted phase boundaries are shown in Fig. 6, and the PFC simulations agree quantitatively well with the theoretical predictions.

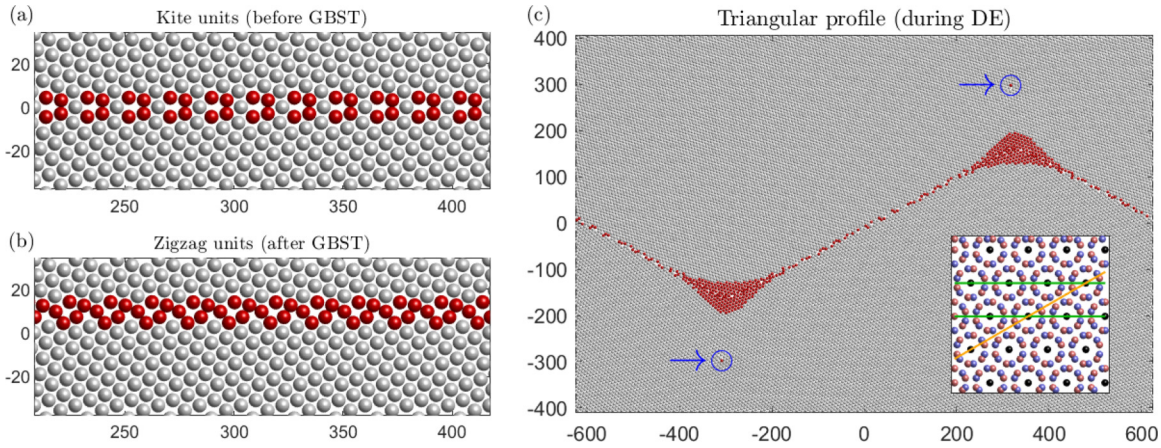


FIG. 5. (a) Kite and (b) zigzag units are observed before and after GBST. The reddish color indicates the grain boundary regions. (c) The triangular grain boundary profile is discovered during the DE phase. The dislocations highlighted with blue circles are emitted from the cusps. The inset shows the dichromatic CSL of the bicrystal structure of our interest, and planes of the CSL are shown in lines.

## IV. CONCLUSIONS

In summary, we have proposed a theoretical framework for the morphological evolution of a grain boundary subject to applied lateral strains. There is not only the grain boundary energy but also an elastic energy associated with grain boundaries. The elastically softer grain boundary enables lattice relaxations of nearby grains, which promotes the instability. In addition, the inclusion of the washboard-type potential due to the atomistic details of the CSL gives rise to two interesting outcomes of the grain boundary evolution. The proposed theory is validated by PFC simulations. Not only is the dispersion relation in good agreement with the proposed theory, but also two possible phases, namely, the GBST and DE, are observed in PFC simulations.

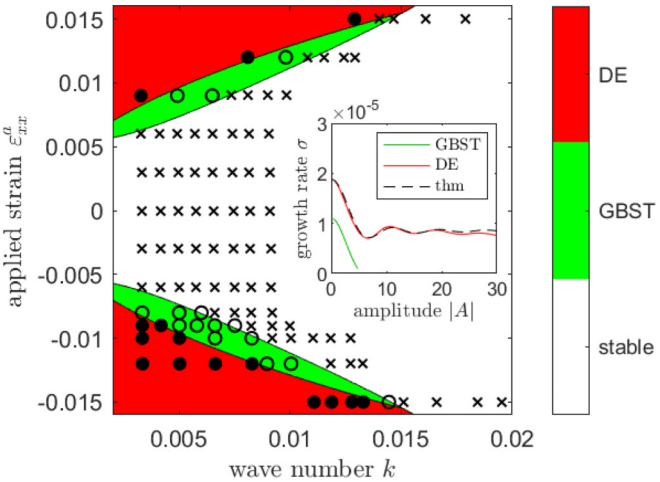


FIG. 6. Phase diagram for the grain boundary instability. Theoretical predictions for the stable regime, the GBST regime, and the DE regime in the $(\varepsilon^a_{xx}, k)$ parameter space are shown in white, green, and red, respectively. PFC simulation results are shown in crosses for the stable regime, empty circles for the GBST regime, and solid circles for the DE regime. The inset shows the amplitude-dependent growth rate for GBST and DE from the PFC simulations (solid lines). The corresponding theoretical predictions based on the washboard potential due to the CSL are plotted in dashed lines.

The study of grain boundaries under stresses is an active area of research; for example, to name just a few recent efforts, there have been attempts to understand shear strain relaxation at the grain boundary [38], lattice transformation in grain boundary migration [39], and diffusional relaxations at the grain boundaries [40]. Such an understanding of the response of grain boundaries to applied stresses is important to understand the high-temperature deformation behavior such as creep and to understand the deformation mechanisms in nanomaterials at lower temperatures. In this context, the current model and PFC simulations which study the transverse loading of grain boundaries are important, and the simulations have the potential to be extended to more practical geometries such as triple junctions and other systems such as grain boundaries with impurity segregation.

## ACKNOWLEDGMENTS

M.-W.L. and K.-A.W. acknowledge the support of the Ministry of Science and Technology, Taiwan (Grants No. MOST 109-2112-M-007-005 and No. MOST 110-2112-M-007-003), and support from the National Center for Theoretical Sciences, Taiwan.

## APPENDIX A: INHOMOGENEOUS STRAIN FIELDS INDUCED BY A GRAIN BOUNDARY OF A SINUSOIDAL PROFILE

For a grain boundary of a sinusoidal profile, $y_{gb}(x) = A\,e^{ikx} + \text{c.c.}$, the strain fields in nearby solids at mechanical equilibrium consist of the uniform applied strain field $\varepsilon^a_{\alpha\beta}$ and an inhomogeneous strain field of the corresponding $k$ mode,

$$\varepsilon_{\alpha\beta}(x, y) = \varepsilon^a_{\alpha\beta} + [\tilde{\varepsilon}_{\alpha\beta}(y)e^{ikx} + \text{c.c.}], \tag{A1}$$

where the uniform applied strain field follows $\varepsilon^a_{yy} = -\nu\varepsilon^a_{xx}$ and $\varepsilon^a_{xy} = 0$ for a given Poisson ratio $\nu$. Consequently, the mechanical equilibrium conditions are given by

$$-\tilde{\partial}_\alpha\tilde{\sigma}_{\alpha\beta}(y) = 0, \qquad \text{within solid grains} \tag{A2}$$

$$\Delta\tilde{\sigma}_{yy} = 0, \qquad \text{along the interface at } y = 0 \tag{A3}$$

$$\tilde{\sigma}_{xy} - ikA\bar{\sigma}_{xx} = \mu b\Delta\tilde{u}_x, \qquad \text{along the interface at } y = 0, \tag{A4}$$

where $\bar{\sigma}_{xx} = E\varepsilon^a_{xx}$, $\tilde{\partial}_\alpha \equiv (ik, \frac{d}{dy})$, and $\bar{\sigma}_{\alpha\beta}$ and $\tilde{\sigma}_{\alpha\beta}$ denote the homogeneous mode and the $k$ mode of $\sigma_{\alpha\beta}$, respectively. By substituting the constitutive equation of isotropic materials, $\sigma_{\alpha\beta} = \lambda\varepsilon_{\xi\xi}\delta_{\alpha\beta} + 2\mu\varepsilon_{\alpha\beta}$, into Eq. (A2) and the relation between strain and displacement, $\varepsilon_{\alpha\beta} = \frac{1}{2}(\frac{\partial u_\beta}{\partial r_\alpha} + \frac{\partial u_\alpha}{\partial r_\beta})$, the equations for the displacement field $\tilde{u}_\alpha$ are obtained accordingly,

$$(\lambda + \mu)\tilde{\partial}_\beta\tilde{\partial}_\xi\tilde{u}_\xi + \mu\tilde{\partial}_\alpha\tilde{\partial}_\alpha\tilde{u}_\beta = 0, \tag{A5}$$

which leads to the Laplace equation of bulk strain, $\tilde{\partial}_\alpha\tilde{\partial}_\alpha\tilde{\varepsilon}_B = 0$, where $\tilde{\varepsilon}_B \equiv \tilde{\varepsilon}_{\alpha\alpha}$.

Because the influence due to a curved grain boundary is negligible at a long distance, we can readily derive the formalism of $\tilde{\varepsilon}_B$,

$$\tilde{\varepsilon}_B(y_\pm) = B_\pm e^{\mp ky_\pm}, \tag{A6}$$

where $B_\pm$ are constants depending on boundary condition, and $y_+$ and $y_-$ are the $y$ coordinates in solids above and below the grain boundary, respectively. The analytical form of $\tilde{\varepsilon}_B$ allows us to simplify Eq. (A5),

$$(\lambda + \mu)\tilde{\partial}_\beta(B_\pm e^{\mp ky_\pm}) + \mu\left[\left(-k^2 + \frac{d^2}{dy_\pm^2}\right)\tilde{u}_\beta(y_\pm)\right] = 0. \tag{A7}$$

The resulting equations lead to

$$\tilde{u}_\beta(y_\pm) = \left[\tilde{v}^\pm_\beta \pm \left(\frac{\lambda + \mu}{2\mu}\right)B_\pm k^{-1}q^\pm_\beta y_\pm\right]e^{\mp ky_\pm}, \tag{A8}$$

where $\tilde{v}^\pm_\beta$ are constants which are determined by boundary conditions and $q^\pm_\beta = (ik, \mp k)$. Note that due to the symmetry of a sinusoidal profile $(x, y) \to (x + \pi/k, -y)$, one expects that $\tilde{v}^+_x = -\tilde{v}^-_x$ and $\tilde{v}^+_y = \tilde{v}^-_y$. By comparing Eq. (A8) with Eq. (A6), we can express $B_\pm$ in terms of $q^\pm_\alpha$ and $\tilde{v}^\pm_\alpha$,

$$B_\pm = \left(\frac{2\mu}{\lambda + 3\mu}\right)q^\pm_\alpha\tilde{v}^\pm_\alpha = \pm\left(\frac{2\mu}{\lambda + 3\mu}\right)(ik\tilde{v}^+_x - k\tilde{v}^+_y), \tag{A9}$$

so one obtains $B_+ = -B_-$.

The stress $\tilde{\sigma}_{yy}$ at the interface $y_\pm = 0$ can be readily expressed in terms of $\tilde{v}^+_\alpha$,

$$\tilde{\sigma}_{yy}(y_\pm = 0) = \pm\lambda B_+ \mp 2\mu\left[k\tilde{v}^+_y + \left(\frac{\lambda + \mu}{2\mu}\right)B_+\right]. \tag{A10}$$

Then, by substituting the equation above into Eq. (A3), one obtains that

$$\tilde{v}^+_y = -\left(\frac{\mu}{\lambda + 2\mu}\right)i\tilde{v}^+_x. \tag{A11}$$

Also, the shear stress at the interface is

$$\tilde{\sigma}_{xy}(y_\pm = 0) = -2\mu\left(\frac{\lambda + \mu}{\lambda + 2\mu}\right)k\tilde{v}^+_x = -\frac{1}{2}Ek\tilde{v}^+_x. \tag{A12}$$

$\tilde{v}^+_x$ can be solved readily by substituting the above equation into Eq. (A4), where we get

$$-\tfrac{1}{2}Ek\tilde{v}^+_x - ikAE\varepsilon^a_{xx} = 2\mu b\tilde{v}^+_x, \tag{A13}$$

and

$$\tilde{v}^+_x = \frac{-2iA\varepsilon^a_{xx}}{1 + 4\mu b/Ek}. \tag{A14}$$

Finally, we arrive at the analytical formalism of the stress field as shown in Eq. (5),

$$\varepsilon_{xx}(y_\pm) = \varepsilon^a_{xx} \pm \left(\frac{2kA\varepsilon^a_{xx}}{1 + 4\mu b/Ek}\right)\left[1 \mp \left(\frac{E}{4\mu}\right)ky_\pm\right]e^{\mp ky_\pm}e^{ikx} + \text{c.c.}, \tag{A15}$$

which is then used to compute the free energy density difference across the grain boundary and the corresponding growth rate of perturbation.

## APPENDIX B: NONLINEAR EQUATION OF AMPLITUDE EVOLUTION

To derive the evolution equation of amplitude $A$, we first make a Fourier transform of Eq. (7),

$$\frac{dA}{dt} = \frac{1}{L_x}\int_0^{L_x}\left(\frac{\partial y_{gb}}{\partial t}\right)e^{-ikx}\,dx = -\frac{\Gamma}{L_x}\int_0^{L_x}\left(\Delta f_{el} + \frac{\delta F_{\text{int}}}{\delta y_{gb}}\right)e^{-ikx}\,dx, \tag{B1}$$

where $L_x = 2\pi/k$. The integral of the first term is readily obtained as discussed in Appendix A. A more compact form of the integral of the second term is obtained by employing the assumed sinusoidal profile of the grain boundary, $y_{gb}(x) = Ae^{ikx} + \text{c.c.}$:

$$\begin{aligned}
&\frac{1}{L_x}\int_0^{L_x}\left(\frac{\delta F_{\text{int}}}{\delta y_{gb}}\right)e^{-ikx}\,dx \\
&= \frac{1}{L_x}\int_0^{L_x}\left[\frac{\partial f_{\text{int}}}{\partial y_{gb}} - \frac{\partial}{\partial x}\left(\frac{\partial f_{\text{int}}}{\partial y'_{gb}}\right)\right]e^{-ikx}\,dx \\
&= \frac{1}{L_x}\int_0^{L_x}\left[\frac{\partial f_{\text{int}}}{\partial y_{gb}} + ik\left(\frac{\partial f_{\text{int}}}{\partial y'_{gb}}\right)\right]e^{-ikx}\,dx \\
&= \frac{1}{L_x}\int_0^{L_x}\left[\left(\frac{\partial f_{\text{int}}}{\partial y_{gb}}\right)\left(\frac{\partial y_{gb}}{\partial A^*}\right) + \left(\frac{\partial f_{\text{int}}}{\partial y'_{gb}}\right)\left(\frac{\partial y'_{gb}}{\partial A^*}\right)\right]dx \\
&= \frac{\partial}{\partial A^*}\left[\frac{1}{L_x}\int_0^{L_x} f_{\text{int}}\,dx\right] \\
&= \frac{\partial\bar{f}_{\text{int}}(A, A^*)}{\partial A^*},
\end{aligned} \tag{B2}$$

where $A^*$ is the complex conjugate of $A$, $f_{\rm int} = \gamma(y_{gb})\sqrt{1+(y'_{gb})^2}$, and $\bar{f}_{\rm int} = \frac{1}{L_x}\int_0^{L_x} f_{\rm int}\, dx$. For the assumed interfacial energy $\gamma(y_{gb}) = \gamma_0 + \gamma_1 \cos(2\pi y_{gb}/L_{cs})$, the analytical form of averaged interfacial energy is determined:

$$\begin{aligned}\bar{f}_{\rm int} &= \frac{1}{L_x}\int_0^{L_x}\left\{\gamma_0+\gamma_1\cos\left[\frac{4\pi|A|}{L_{cs}}\cos(kx+\phi)\right]\right\}\sqrt{1+4k^2|A|^2\sin^2(kx+\phi)}\,dx\\ &= \frac{1}{2\pi}\int_0^{2\pi}\left[\gamma_0+\gamma_1\cos\left(\frac{4\pi|A|}{L_{cs}}\cos z\right)\right](1+2k^2|A|^2\sin^2 z)\,dz+\mathcal{O}(k|A|)^4\\ &\simeq \gamma_0(1+k^2|A|^2)+\gamma_1 J_0(\eta)-\gamma_1 k^2|A|\left(\frac{L_{cs}}{2\pi}\right)J_0'(\eta),\end{aligned} \tag{B3}$$

where $A = |A|e^{i\phi}$, $z = kx+\phi$, $\eta = 4\pi|A|/L_{cs}$, and $J_0(x)$ is the zeroth-order Bessel function. The derivative of $\bar{f}_{\rm int}$ with respect to $A^*$ is readily solved:

$$\begin{aligned}\frac{\partial \bar{f}_{\rm int}}{\partial A^*} &= \frac{1}{2}e^{i\phi}\left(\frac{d\bar{f}_{\rm int}}{d|A|}\right)\\ &= e^{i\phi}\left\{\gamma_0 k^2|A|+\gamma_1\left(\frac{2\pi}{L_{cs}}\right)J_0'(\eta)-\gamma_1 k^2\left(\frac{L_{cs}}{4\pi}\right)\left[J_0'(\eta)+\left(\frac{4\pi|A|}{L_{cs}}\right)J_0''(\eta)\right]\right\}\\ &= \left\{\gamma_0 k^2+\gamma_1\left(\frac{2\pi}{L_{cs}}\right)^2\left[\frac{2J_0'(\eta)}{\eta}\right]-\gamma_1 k^2\left[\frac{J_0'(\eta)}{\eta}+J_0''(\eta)\right]\right\}|A|e^{i\phi}\\ &= \left[\gamma_0 k^2-\gamma_1\left(\frac{2\pi}{L_{cs}}\right)^2[J_0(\eta)+J_2(\eta)]+\gamma_1 k^2 J_0(\eta)\right]A,\end{aligned} \tag{B4}$$

where we use the Bessel differential equation, $x^2J_0''(x)+xJ_0''(x)+x^2J_0(x)=0$, and the recurrence relation of Bessel functions, $2J_0'(x) = J_{-1}(x)-J_1(x) = -2J_1(x)$ and $2J_1(x)/x = -[J_0(x)+J_2(x)]$, to simplify the calculation. Combining Eqs. (6), (B1), (B2), and (B4), we obtain the nonlinear evolution equation for the amplitude of the grain boundary:

$$\frac{dA}{dt} \simeq -\Gamma\left\{-\frac{4E\,\varepsilon_{xx}^{a\,2}\,k}{1+4\mu_1/Ek}+[\gamma_0+\gamma_1 J_0(\eta)]k^2-\gamma_1\left(\frac{2\pi}{L_{cs}}\right)^2[J_0(\eta)+J_2(\eta)]\right\}A. \tag{B5}$$


[1] A. Sutton and R. Balluffi, *Interfaces in Crystalline Materials*, Monographs on the physics and chemistry of materials (Clarendon Press, Oxford, 1995).

[2] M. Lagos, Elastic Instability of Grain Boundaries and the Physical Origin of Superplasticity, Phys. Rev. Lett. **85**, 2332 (2000).

[3] M. Lagos, Theory of superplasticity in polycrystalline materials: Stress-induced structural instabilities of grain boundaries, Phys. Rev. B **71**, 224117 (2005).

[4] J. P. Liebig, M. Makovi, E. Spiecker, M. Göken, and B. Merle, Grain boundary mediated plasticity: A blessing for the ductility of metallic thin films?, Acta Mater. **215**, 117079 (2021).

[5] R. Cano-Crespo, B. M. Moshtaghioun, D. G. García, A. D. Rodríguez, C. Retamal, and M. Lagos, Mechanical instability of stressed grain boundaries during plastic deformation of zirconium carbide, J. Eur. Ceram. Soc. **36**, 2235 (2016).

[6] M. Lagos and C. Retamal, Grain dynamics and plastic properties of highly refined materials, Phys. Scr. **82**, 065603 (2010).

[7] D. Srolovitz, On the stability of surfaces of stressed solids, Acta Metall. **37**, 621 (1989).

[8] B. J. Spencer, P. W. Voorhees, and S. H. Davis, Morphological instability in epitaxially strained dislocationfree solid films: Linear stability theory, J. Appl. Phys. **73**, 4955 (1993).

[9] X. Li, Thermodynamic analysis on the stability and evolution mechanism of self-assembled quantum dots, Appl. Surf. Sci. **256**, 4023 (2010).

[10] C. G. Gamage and Z.-F. Huang, Nonlinear dynamics of island coarsening and stabilization during strained film heteroepitaxy, Phys. Rev. E **87**, 022408 (2013).

[11] G. K. Dixit and M. Ranganathan, Modeling elastic anisotropy in strained heteroepitaxy, J. Phys.: Condens. Matter **29**, 375001 (2017).

[12] R. J. Asaro and W. A. Tiller, Interface morphology development during stress corrosion cracking: Part I. Via surface diffusion, Metall. Mater. Trans. B **3**, 1789 (1972).

[13] M. A. Grinfeld, The stress driven instability in elastic crystals: Mathematical models and physical manifestations, J. Nonlinear Sci. **3**, 35 (1993).

[14] N. Sridhar, J. M. Rickman, and D. J. Srolovitz, Microstructural stability of stressed lamellar and fiber composites, Acta Mater. **45**, 2715 (1997).

[15] K. R. Elder, M. Katakowski, M. Haataja, and M. Grant, Modeling Elasticity in Crystal Growth, Phys. Rev. Lett. **88**, 245701 (2002).

[16] K. R. Elder and M. Grant, Modeling elastic and plastic deformations in nonequilibrium processing using phase field crystals, Phys. Rev. E **70**, 051605 (2004).
[17] W. Bollmann, *Crystal Defects and Crystalline Interfaces* (Springer, Berlin, Heidelberg, 1970).
[18] H. Gao and W. D. Nix, Surface roughening of heteroepitaxial thin films, Annu. Rev. Mater. Sci. **29**, 173 (1999).
[19] S. Balibar, H. Alles, and A. Y. Parshin, The surface of helium crystals, Rev. Mod. Phys. **77**, 317 (2005).
[20] K.-A. Wu and P. W. Voorhees, Phase field crystal simulations of nanocrystalline grain growth in two dimensions, Acta Mater. **60**, 407 (2012).
[21] Z. T. Trautt, A. Adland, A. Karma, and Y. Mishin, Coupled motion of asymmetrical tilt grain boundaries: Molecular dynamics and phase field crystal simulations, Acta Mater. **60**, 6528 (2012).
[22] A. Adland, A. Karma, R. Spatschek, D. Buta, and M. Asta, Phase-field-crystal study of grain boundary premelting and shearing in bcc iron, Phys. Rev. B **87**, 024110 (2013).
[23] S.-C. Lin, M.-W. Liu, M. P. Gururajan, and K.-A. Wu, Modified Young's equation for equilibrium dihedral angles of grain boundary grooves in thin films at the nanoscale, Acta Mater. **102**, 364 (2016).
[24] K. McReynolds, K.-A. Wu, and P. Voorhees, Grain growth and grain translation in crystals, Acta Mater. **120**, 264 (2016).
[25] M. Seymour and N. Provatas, Structural phase field crystal approach for modeling graphene and other two-dimensional structures, Phys. Rev. B **93**, 035447 (2016).
[26] A. Yamanaka, K. McReynolds, and P. W. Voorhees, Phase field crystal simulation of grain boundary motion, grain rotation and dislocation reactions in a bcc bicrystal, Acta Mater. **133**, 160 (2017).
[27] J. Li, B. Ni, T. Zhang, and H. Gao, Phase field crystal modeling of grain boundary structures and growth in polycrystalline graphene, J. Mech. Phys. Solids **120**, 36 (2018).
[28] D. Taha, S. K. Mkhonta, K. R. Elder, and Z.-F. Huang, Grain Boundary Structures and Collective Dynamics of Inversion Domains in Binary Two-Dimensional Materials, Phys. Rev. Lett. **118**, 255501 (2017).
[29] J. Berry, M. Grant, and K. R. Elder, Diffusive atomistic dynamics of edge dislocations in two dimensions, Phys. Rev. E **73**, 031609 (2006).
[30] J. Berry, K. R. Elder, and M. Grant, Melting at dislocations and grain boundaries: A phase field crystal study, Phys. Rev. B **77**, 224114 (2008).
[31] P. Y. Chan, G. Tsekenis, J. Dantzig, K. A. Dahmen, and N. Goldenfeld, Plasticity and Dislocation Dynamics in a Phase Field Crystal Model, Phys. Rev. Lett. **105**, 015502 (2010).
[32] D. L. Olmsted, D. Buta, A. Adland, S. M. Foiles, M. Asta, and A. Karma, Dislocation-Pairing Transitions in Hot Grain Boundaries, Phys. Rev. Lett. **106**, 046101 (2011).
[33] J. Berry, N. Provatas, J. Rottler, and C. W. Sinclair, Phase field crystal modeling as a unified atomistic approach to defect dynamics, Phys. Rev. B **89**, 214117 (2014).
[34] M. Salvalaglio, A. Voigt, Z.-F. Huang, and K. R. Elder, Mesoscale Defect Motion in Binary Systems: Effects of Compositional Strain and Cottrell Atmospheres, Phys. Rev. Lett. **126**, 185502 (2021).
[35] J. Mellenthin, A. Karma, and M. Plapp, Phase-field crystal study of grain-boundary premelting, Phys. Rev. B **78**, 184110 (2008).
[36] M.-W. Liu and K.-A. Wu, Investigation of surface/bulk stresses of nanoparticles with diffusive interfaces using the phase field crystal model, Phys. Rev. B **96**, 214106 (2017).
[37] K.-A. Wu and P. W. Voorhees, Stress-induced morphological instabilities at the nanoscale examined using the phase field crystal approach, Phys. Rev. B **80**, 125408 (2009).
[38] N. Combe, F. Mompiou, and M. Legros, Multiple coupling modes to relax shear strain during grain boundary migration, Acta Mater. **218**, 117222 (2021).
[39] B. Li and J. Leung, Lattice transformation in grain boundary migration via shear coupling and transition to sliding in face-centered-cubic copper, Acta Mater. **215**, 117127 (2021).
[40] F. Delannay, The role of grain boundary mobility in diffusional deformation, J. Mech. Phys. Solids **154**, 104512 (2021).